

# Lawrence Berkeley National Laboratory

## Recent Work

### Title

BETA-DEIAYED TWO-PROTON DECAYS OF 22AI AND 26P

### Permalink

<https://escholarship.org/uc/item/4bd342v7>

### Author

Cable, M.D.

### Publication Date

1984-06-01



# Lawrence Berkeley Laboratory

UNIVERSITY OF CALIFORNIA

RECEIVED  
LAWRENCE  
BERKELEY LABORATORY

JUL 24 1984

LIBRARY AND  
DOCUMENTS SECTION

Submitted to Physical Review C

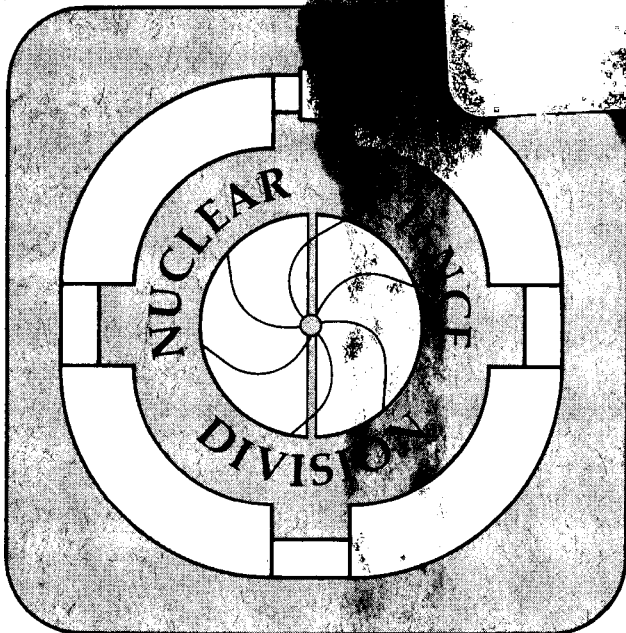
BETA-DELAYED TWO-PROTON DECAYS OF  $^{22}\text{Al}$  AND  $^{26}\text{P}$

M.D. Cable, J. Honkanen, E.C. Schloemer,  
M. Ahmed, J.E. Reiff, Z.Y. Zhou, and J. Cerny

June 1984

TWO-WEEK LOAN COPY

*This is a Library Circulating Copy  
which may be borrowed for two weeks*



## **DISCLAIMER**

This document was prepared as an account of work sponsored by the United States Government. While this document is believed to contain correct information, neither the United States Government nor any agency thereof, nor the Regents of the University of California, nor any of their employees, makes any warranty, express or implied, or assumes any legal responsibility for the accuracy, completeness, or usefulness of any information, apparatus, product, or process disclosed, or represents that its use would not infringe privately owned rights. Reference herein to any specific commercial product, process, or service by its trade name, trademark, manufacturer, or otherwise, does not necessarily constitute or imply its endorsement, recommendation, or favoring by the United States Government or any agency thereof, or the Regents of the University of California. The views and opinions of authors expressed herein do not necessarily state or reflect those of the United States Government or any agency thereof or the Regents of the University of California.

Beta-delayed Two-proton Decays of  $^{22}\text{Al}$  and  $^{26}\text{P}$ 

M. D. Cable, J. Honkanen<sup>+</sup>, E. C. Schloemer, M. Ahmed,  
J. E. Reiff, Z. Y. Zhou<sup>++</sup>, and Joseph Cerny

Department of Chemistry and  
Lawrence Berkeley Laboratory  
University of California  
Berkeley, California 94720

June, 1984

PACS Numbers: 23.40.Hc

Abstract

Beta-delayed two-proton radioactivity has been observed for the two nuclei,  $^{22}\text{Al}$  and  $^{26}\text{P}$ . Proton-proton coincidence experiments performed at small and large angles show that the dominant two-proton emission mechanism is a sequential process. Decay schemes have been determined for each isotope.

RADIOACTIVITY:  $^{22}\text{Al}$  from  $^{24}\text{Mg}(^3\text{He}, p4n)$  and  $^{26}\text{P}$  from  $^{28}\text{Si}(^3\text{He}, p4n)$ ; measured beta-delayed two-protons; deduced decay schemes and states in  $^{21}\text{Na}$ ,  $^{25}\text{Al}$ .

\*This work was supported by the Director, U.S. Office of Energy Research, Division of Nuclear Physics of the Office of High Energy and Nuclear Physics, and by Nuclear Sciences of the Basic Energy Sciences Program of the U. S. Department of Energy under Contract No. DE-AC03-76SF00098.

## I. Introduction

Beta-delayed two-proton radioactivity is a new decay process originally predicted by Gol'danskii in 1980<sup>1)</sup>. This process involves the relatively slow beta decay of an isotope to an excited state of its daughter which subsequently decays by the rapid emission of two protons. In particular, Gol'danskii predicted that should the then unknown isotopes  $^{22}\text{Al}$  and  $^{26}\text{P}$  exist, they would be prime candidates to exhibit this decay mode. Recent studies of the beta-delayed proton decay of these two isotopes<sup>2,3)</sup> showed not only that they do exist, but provided a measurement of the masses of the lowest  $T=2$  analog states in the beta decay daughters which are fed by superallowed beta decay. These states were thus shown to be unbound to the emission of two protons, as predicted, and subsequent proton-proton coincidence experiments<sup>4,5)</sup> detected the first known cases of beta-delayed two-proton radioactivity.

Both  $^{22}\text{Al}$  and  $^{26}\text{P}$  exhibit this decay mode. Figures 1 and 2 show the similar decay schemes for each of these odd-odd,  $T_z = -2$  isotopes. Using the  $^{22}\text{Al}$  decay as an example,  $^{22}\text{Al}$  will be referred to as the precursor,  $^{22}\text{Mg}$  as the emitter, and  $^{21}\text{Na}$  and  $^{20}\text{Ne}$  as the proton and two-proton daughters, respectively. Due to the relatively large superallowed beta decay branch to the  $T = 2$  analog state in the emitter nucleus, decay modes involving this state are most readily observed experimentally, and unless explicitly stated otherwise, all decay branches discussed in this work will involve the analog state.

It can be seen from Figs. 1 and 2 that a variety of decays of the analog states are energetically possible. Particle emissions in the forms of  $\alpha$ , p, or 2p decay all have several MeV of decay energy and are all expected to contribute to the total decay. Alpha particles of the energies expected are not observable in the experimental work to be described and will not be discussed. One notable difference between the  $^{22}\text{Al}$  and  $^{26}\text{P}$  decays is that  $^2\text{He}$  emission (a two-proton emission mechanism discussed further below) is spin-parity forbidden for the  $^{26}\text{P}$  beta-delayed two-proton branch ending in the  $^{24}\text{Mg}$  ground state. This makes a comparison of these decays especially useful for a characterization of two-proton emission mechanisms. Beta-delayed proton decay of both  $^{22}\text{Al}$  and  $^{26}\text{P}$  has been discussed in Refs. 2 and 3 and results of the measurements, such as the masses of the analog states, will be used here without describing the experimental work in detail. The focus of this paper will be to summarize all the experimental work on the beta-delayed two-proton decay branch and to relate this to possible decay mechanisms for two-proton emission.

## II. Two-Proton Emission Mechanisms

Since two-proton emission from a relatively long-lived state such as these  $T = 2$  analog states (particle emission is slowed because it is isospin-forbidden) has never been observed, the question of how these protons will leave the nucleus is an interesting one. Much of the early theoretical work of Gol'danskii on direct two-proton radioactivities<sup>6)</sup> is applicable here. Drawing on this as background, several possible decay mechanisms will be presented.

One possibility is that the protons will leave the nucleus coupled to a  $^1S_0$  configuration. This process will be referred to as  $^2\text{He}$  emission. The virtual state,  $^2\text{He}$ , has been studied in reaction work (for example, Ref. 7 or 8) and for our purposes, can be thought of as a proton pair penetrating the Coulomb and angular momentum barriers of the nucleus with a virtual energy,  $\epsilon$ , shared between the protons. This center-of-mass energy of the proton pair then "returns" at some distance from the nucleus as kinetic energy of the protons which are now correlated at small angles. For simplicity, this discussion (in particular, the Monte Carlo simulations described below) will assume this break-up occurs well outside the Coulomb and angular momentum barriers. This simplification has very little effect on the observable experimental properties.

For  $^2\text{He}$  emission, momentum and energy conservation give the following expression for the summed laboratory energy of the two protons:

$$E^L = \frac{mE_{\text{cm}} + 2m_p \epsilon + \epsilon^2}{m + 2m_p} \quad (1)$$

where

- $E_{\text{cm}}$  = center-of-mass decay energy for the two protons,
- $\epsilon$  = relative energy of the two protons (sometimes called the break-up energy),
- $m_p$  = mass of proton, and
- $m$  = mass of two-proton daughter (for  $^{22}\text{Al}$ , mass of  $^{20}\text{Ne}$ ).

The quantity  $\epsilon$  is determined by the nucleon-nucleon interaction of the proton pair (commonly referred to as the final state interaction) and is expected from reaction work (again, for example, Ref. 7 or 8) to appear as a distribution with a maximum value of  $\sim 500$  keV and a FWHM of  $\sim 600$  keV.

Given a value for  $\epsilon$ , the kinematic expressions for laboratory energies and angles of the protons are a standard problem solved in many texts such as Ref. 9 or 10. For the purposes of this discussion, it is sufficient to summarize this calculation with the expression:

$$\cos\eta = \frac{E_1^L + E_2^L - 2\epsilon}{2\sqrt{E_1^L E_2^L}} \quad (2)$$

where

$\eta$  = the relative laboratory angle between the protons,

and  $E_1^L, E_2^L$  = individual proton laboratory energies ( $E_1^L + E_2^L = E^L$ ).

$\eta$  is maximized for  $E_1^L = E_2^L$ , and this is also expected to be its most probable value; therefore, the individual proton spectrum from  ${}^2\text{He}$  emission should be a distribution, symmetric about  $E_1^L = E_2^L$  with its shape determined by the final state interaction (distribution in  $\epsilon$ ) and also by the detector efficiency variation as a function of  $\eta$ . The expected appearance of the  ${}^2\text{He}$  spectra in the laboratory is calculated through Monte Carlo simulations presented below, after the detector systems have been described.



Another class of decay mechanisms besides  ${}^2\text{He}$  emission will be categorically referred to as uncoupled mechanisms. An uncoupled mechanism can be thought of as two protons independently leaving the nucleus with a time,  $\Delta t$ , between the first and second emission. If  $\Delta t$  is long enough for the formation of an intermediate state of the proton daughter nucleus, then this process will be referred to as a sequential emission. The alternative case ( $\Delta t \ll 10^{-21}$  s) will be referred to as pre-equilibrium emission.

Sequential emission is in many ways similar to a gamma ray cascade. Two protons, each with a discrete decay energy dependent upon the intermediate state energy, will be emitted. For sequential emissions where neither proton has  $\ell=0$  and the intermediate state spin is not  $1/2$ , angular correlations are expected. For protons, however, these angular correlations are not expected to be large ( $< 10\text{-}20\%$  effect from calculations based on methods described in Ref. 11) and for most of this work will not be discussed, since the experiments described below could not distinguish between weakly correlated distributions and isotropic emission. As in gamma ray cascades, the second proton is emitted from a recoiling nucleus and the conversion from center-of-mass to laboratory energies must account for this fact. Unlike gamma rays, however, protons are relatively massive and this recoil effect is quite large; it will, in fact, be a major factor in identification of a two-proton decay as a sequential emission.

For sequential emission, expressions for the laboratory energies of the two individual protons are:

$$E_1^L = \left( \frac{m_1}{m_2} \right) E_1$$

$$E_2^L = \left( \frac{m}{m_1} \right) (E_{cm} - E_1) + \frac{E_1 (m_p)^2}{(m_1)(m_2)} - \frac{2m_p \cos\theta}{m_1} \sqrt{\frac{mE_1(E_{cm} - E_1)}{m_2}} \quad (3)$$

where symbols not in equations 1 or 2 are defined as:

$m_1$  = mass of intermediate state in the proton daughter

(for  $^{22}\text{Al}$ , mass of  $^{21}\text{Na}^*$ ),

$m_2$  = mass of two-proton emitter state

(for  $^{22}\text{Al}$ , mass of  $^{22}\text{Mg}^*$ ),

$E_1$  = center of mass decay energy for proton one,

$\theta$  = center of mass angle between the protons.

It can be seen that the first proton in sequential emission has the usual laboratory energy calculated as in single proton emission but that the second proton laboratory energy is a function of  $\theta$ . Again, Monte Carlo simulations of expected observable proton spectra will be presented below.

A detailed description of pre-equilibrium emission ( $\Delta t$  short) of two protons would involve a knowledge of the evolution of the nucleus following the emission of the first proton. This makes such a treatment quite difficult and we shall only discuss the qualitative features of the relatively simple, limiting case of  $\Delta t=0$ . For this

case, if possible spin-dependent angular correlations are negligibly small as in sequential emission and ignoring barrier penetrabilities, then phase space limitations will determine the proton energy spectrum; the appropriate kinematics are readily soluble. Individual proton spectra for the  $\Delta t=0$  case will again, as in  ${}^2\text{He}$  emission, consist of a continuum of proton energies with equal  $p_1$  and  $p_2$  energies being the most probable case. Unlike  ${}^2\text{He}$  emission, however, these protons are not restricted to small angles and there is an angular dependence for their laboratory energies similar to that of sequential emission. Monte Carlo simulations for the  $\Delta t=0$  case of pre-equilibrium emission will be discussed below.

### III. Experimental Method and Monte Carlo Simulations

${}^{22}\text{Al}$  ( $t_{1/2} \sim 70$  ms) and  ${}^{26}\text{P}$  ( $t_{1/2} \sim 20$  ms) were produced via the  ${}^{24}\text{Mg}({}^3\text{He}, p4n){}^{22}\text{Al}$  and  ${}^{28}\text{Si}({}^3\text{He}, p4n){}^{26}\text{P}$  reactions with 110 MeV  ${}^3\text{He}^{+2}$  beams of 3-7  $\mu\text{A}$  intensities from the Lawrence Berkeley Laboratory's 88-Inch Cyclotron. Recoiling product nuclei were stopped in  $\sim 1.3$  atm helium and transported to a detector chamber with the helium jet apparatus shown schematically in Fig. 3. NaCl was used as an additive to improve speed and transport efficiency through the 70 cm (1.3 mm i.d.) capillary. Transported activity was collected on a catcher wheel to form a source for particle spectroscopy with the solid state telescopes described below. Long-lived beta activities were reduced by a slow rotation of the catcher wheel with further removal of beta background accomplished by magnets and collimators.

All data were recorded event by event on a ModComp Classic computer using the data acquisition and analysis program, CHAOS<sup>12)</sup>, enabling use of several software particle identification techniques.

Figure 4 is a schematic diagram of the "small angle" detector system. This system was a three element semiconductor particle telescope (14-31 $\mu$ m  $\Delta E1$ , 155-170 $\mu$ m  $\Delta E2$ , 500-1000 $\mu$ m E) with each circular  $\Delta E$  detector fabricated such that the surface contact on one side was divided on the center-line. This effectively produced two detectors on the same silicon wafer which will be referred to as "left" (L) and "right" (R) detectors. Such an arrangement could detect low energy protons (typically  $\sim 1.0$ -4.5 MeV) as  $\Delta E1$ ,  $\Delta E2$  coincidences in either the left or right sides or high energy protons (typically 4.7-9.0 MeV) as  $\Delta E1$ ,  $\Delta E2$ , E coincidences. Most importantly, particle-identified proton-proton coincidences could be observed between the left and right sides with a timing resolution typically better than 10 ns (FWHM).

Each two element, low energy telescope (e.g.,  $\Delta E1$ -L and  $\Delta E2$ -L) subtended 4.5% of  $4\pi$  sr and each three element, high energy telescope subtended 1.5% of  $4\pi$  sr (these high energy telescopes share the common, unsplit E detector). Since the left and right telescopes were separated by only a small distance, protons with a relative laboratory angle very close to  $\eta=0^\circ$  could be detected. The largest angle that could be detected was about  $\eta = 70^\circ$ , with the weighted average for the system being  $\eta \sim 45^\circ$ . This arrangement was chosen primarily because a) it is desirable to subtend the largest possible solid

angles in order to increase the sensitivity to these low yield activities as the effective delayed proton cross-sections for  $^{22}\text{Al}$  and  $^{26}\text{P}$  are a few nanobarns and b) a small angle system has the advantage of being able to detect the correlated protons from  $^2\text{He}$  emission as well as the expected approximately isotropic distribution of a sequential emission. Equations 1 and 2 show that for the decay energies involved for  $^2\text{He}$  emission from  $^{22}\text{Al}$  and  $^{26}\text{P}$ , and assuming  $\epsilon \sim 500$  keV, the maximum (and most probable) value of  $n$  occurs at  $n \sim 40^\circ$ ; therefore, this small angle system should be an excellent tool with which to search for either  $^2\text{He}$  or sequential emission.

Monte Carlo simulations of expected observable proton-proton coincidence data for the small angle detector system are shown in Figs. 5 and 6. Figure 5 shows the expected two-proton sum spectrum and the spectrum of the individual protons contributing to the sum, for a sequential two-proton emission mechanism for  $^{22}\text{Al}$ . The specific transition calculated is from the  $T = 2$  analog state in  $^{22}\text{Mg}$  to the first excited state in  $^{20}\text{Ne}$  (to be referred to as the  $^{22}\text{Al} \times$  transition) via a hypothetical intermediate state placed such that the first proton has a 3 MeV center-of-mass decay energy. Perfect detector energy resolution is assumed in order to show laboratory energy changes due solely to kinematic effects. It can be seen that the first proton ( $p_1$ ) is emitted with a well defined, easily calculable laboratory energy as in single proton emission or alpha decay. The second proton ( $p_2$ ), however, has a laboratory energy dependent upon the center-of-mass angle between  $p_1$  and  $p_2$ .

(see Eqn. 3) so that its observed energy appears as a distribution determined by the spread in observable laboratory angles and the relative detection efficiency as a function of angle. (The reader should keep in mind that these detectors subtend large solid angles).

Figure 6 presents the same type of simulation assuming a  ${}^2\text{He}$  emission mechanism. A fixed value of  $\epsilon = 500$  keV was chosen for this example and the assumption was made that the  ${}^2\text{He}$  breakup occurs relatively far from the nucleus (see Section II). These simplifications do not qualitatively affect the spectra obtained. The two-proton sum spectrum is seen to be very similar to that obtained in the calculation for sequential emission (the difference in width of the peaks will not be a strong distinguishing feature due to the individual telescope resolution of  $\sim 50$  keV FWHM); however, the individual proton spectrum is quite different. For  ${}^2\text{He}$  emission, a continuum of individual proton energies centered at  $E_{p_1} = E_{p_2}$  is expected. This distribution is maximized for the most probable emission of  $E_{p_1} = E_{p_2}$  if the detectors are very large. Finite detector size produces a dip at this energy such as that shown in Fig. 6b.

A simulation of pre-equilibrium two-proton emission, for the  $\Delta t=0$  limit described in Section II, produces small angle spectra very similar to those for  ${}^2\text{He}$  emission. The two-proton sum spectrum is a single relatively sharp peak and the individual proton energies are a continuum symmetric about  $E_{p_1} = E_{p_2}$ ; however in this case, the individual proton spectrum is always maximized at  $E_{p_1} = E_{p_2}$ .

A comparison of experimental data to these Monte Carlo simulations for the small angle detector system is presented below and will be shown to be quite useful, but in itself will not provide a conclusive characterization of the two-proton decay mechanism. More two-proton measurements made with a large angle detector system provided additional information; this system will be described next.

Figure 7 shows a schematic diagram of the large angle detector system. This arrangement consisted of two separate telescopes ( $\Delta E1$  20-25  $\mu\text{m}$ ,  $\Delta E2$  200-250  $\mu\text{m}$ ,  $E$  500-1000  $\mu\text{m}$ ). Both single protons and two-proton coincidences could be obtained with this system in the same manner as that described above. The large angle detector system had an average angle of  $\eta = 120^\circ$  between the circular telescopes and subtended 4.5% of  $4\pi$  sr on each side for low energy protons (stopping in  $\Delta E2$ ) and 3.0% of  $4\pi$  sr on each side for high energy protons. This corresponds to a minimum detectable angle of  $\eta = 70^\circ$  and a maximum of  $\eta = 170^\circ$ .

A Monte Carlo simulation for a sequential two-proton emission (as described above) observed with the large angle detector system is shown in Fig. 8. Relative to the small angle data simulated in Fig. 5, it can be seen that for sequential emission a kinematic shift in the laboratory energy of the second proton is expected. This, of course, also causes a shift in the two-proton sum peak. There is also a broadening of the second proton peak due to the larger angular range covered by this system and the faster variation in the  $\cos\theta$  term in Eqn. 3 for this region.

${}^2\text{He}$  emission is not expected to be observable with the large angle detector system. Only much larger values of  $\epsilon$  than those expected from Ref. 7 or 8 will produce a sufficiently large break-up angle for detection; therefore, any two-proton decays observed with this large angle detector system are expected to arise from a mechanism other than  ${}^2\text{He}$  emission.

Simulation of  $\Delta t = 0$  pre-equilibrium two-proton emission, which is not constrained to small angles, produces a two-proton sum peak at virtually the same energy as the shifted sum peak for sequential emission; however, the individual proton spectrum appears the same as at small angles.

To summarize all the mechanisms discussed, nearly identical two-proton sum peaks are expected in small and large angle experiments, with a measurable kinematic shift to higher energies at large angles (except for  ${}^2\text{He}$  emission which will not be observed at large angles). Individual proton spectra vary such that: (a) sequential emission will have discrete energy first and second proton groups with the latter exhibiting the small to large angle kinematic shift; (b)  ${}^2\text{He}$  emission will produce a continuum at small angles and will not be observable at large angles; and (c)  $\Delta t = 0$  pre equilibrium emission will produce a continuum at both large and small angles.

#### IV. Results

Small and large angle measurements were made while bombarding Mg and Si targets in order to produce  ${}^{22}\text{Al}$  and  ${}^{26}\text{P}$ , respectively. Results of these measurements are displayed in Figs. 9-13, many of which represent the summation of several experiments. Summaries



of the observed two-proton sum and individual proton energies are presented in Tables I and II.

For  $^{22}\text{Al}$ , two two-proton groups were observed and are shown in Fig. 9a. The observed two-proton sum energies are presented in Table I. Conversion of these laboratory energies to center-of-mass decay energies is dependent upon the two-proton emission mechanism and also upon details of the detector system, but these two groups can be shown to correspond to two-proton transitions from the  $T=2$  analog state in  $^{22}\text{Mg}$  to the first excited and ground states of  $^{20}\text{Ne}$  (labeled x and g, respectively). Figures 9b and 9c are spectra of the individual protons making up these groups. They are obtained by gating on the indicated two-proton group, producing its "left" and "right" spectra (which are identical within statistics except for minor detector differences) and adding them together. It can be seen that both the x and g individual proton spectra appear to be composed of several discrete groups - the signature of a sequential decay mechanism. For the x group, three intermediate states in the proton daughter are involved, producing three pairs of proton groups ( $p_1$  and  $p_2$ ) labeled  $x_1$ ,  $x_1'$ , etc. Only two intermediate states are readily identified for the g transition. These individual proton group energies are summarized in Table II.

Further evidence of the sequential nature of this decay is seen by a comparison of the small and large angle measurements. Figure 10a shows the two-proton sum spectrum obtained for  $^{22}\text{Al}$  with the large angle detector system; the small and large angle measurements

are overlaid in Fig. 11. This figure clearly shows the kinematic shift of each two-proton group to higher energies, with the magnitude of each shift agreeing very well with that expected from Monte Carlo simulations described above (and also with a simple estimate obtainable from Eqn. 3 using  $45^\circ$  and  $120^\circ$ ). Since it is the second proton energy that is shifted, it is, in principle, possible to identify the order of the decay ( $p_1$  vs  $p_2$ ) by a comparison of the small and large angle individual proton spectra. This works very well for the transitions involved in the g group (see Table II) and readily allows identification of groups  $g_1$  and  $g_2'$  as the first protons. Again, the energy shifts of the second protons agree very well with that expected for a sequential mechanism. A large angle measurement of the individual protons corresponding to the  $^{22}\text{Al } x$  transition, however, produces the poorly resolved spectrum shown in Fig. 10b. This precludes positive identification of the ordering of the proton pairs involved in the  $x$  transition; however, tentative assignments of  $x_1'$ ,  $x_2'$ , and  $x_3'$  as first proton groups can be made. As seen in Table III, (and as is discussed in more detail below) these tentative assignments also constitute a more reasonable decay scheme based on previously observed states in  $^{21}\text{Na}$  than one built upon the alternative orderings.

The appearance of the large angle measurement of the  $^{22}\text{Al } x$  transition shown in Fig. 10b is not fully understood. In general, the large angle measurements have poorer energy resolution than that of the small angle measurements due to a) the poorer intrinsic

resolution of the larger surface area (higher capacitance)  $\Delta E1$  detectors used and b) the kinematic broadening effect exhibited in the Monte Carlo simulations. These effects can be quite important since good energy and particle determinations are important for detection of these nanobarn cross-section proton-proton coincidences in the high background present from beta and alpha particles, neutrons, gamma rays, etc.; however, this does not entirely explain this spectrum. There appears to be a possibility of a contribution from a continuum energy proton distribution, particularly since, as discussed below with respect to the 2p/1p ratio, there seems to be more two-proton events in this measurement than expected from the small angle work. Evidence for such a contribution is not strong, however, and would be difficult to explain, particularly since it is absent at small angles. A comparison of Fig. 9c and 10c also shows that the relative intensities of the  $^{22}\text{Al}$  g1 and g2 proton pairs change. This may be at least partially due to differences in the variations of detector efficiencies with energy for the two detector systems, but may also indicate a stronger angular correlation than the 10-20% upper limit expected from standard calculations (these limits assume intermediate state spins up to 7/2). Both of these features merit further investigation in future work.

Bombardments of Si produced not only the previously observed  $^{22}\text{Al}$  x and g groups (from the  $^{28}\text{Si}(^3\text{He}, \alpha p 4n)^{22}\text{Al}$  reaction) but, additionally, a new two-proton sum group corresponding to the two-proton transition from the  $T = 2$  analog state in  $^{26}\text{Si}$  to the

ground state of  $^{24}\text{Mg}$  and labeled  $^{26}\text{p g}$  in Figs. 12a and 13a. The individual proton spectra corresponding to this group are shown in Figs. 12b and 13b. This group again exhibits the signature of a sequential emission, this time through a single intermediate state in  $^{25}\text{Al}$ . Tables I and II display the observed energies of these groups and show that  $g^1$  is identifiable as the first proton. Kinematic shifts are again as expected from calculation. The expected location of the  $^{26}\text{p x}$  two-proton sum peak is also labeled in Fig. 12a and 13a. This group is too close to the low energy detection threshold, however, to measure reliably. It is only possible to say that some contribution is probably observed, particularly in the large angle measurement.

With the individual proton energies in Table II, the sequence of emissions described above, and the mass excesses of the  $T = 2$  analog states (measured in Refs. 2 and 3), it is possible to determine the mass excesses of the intermediate states in the proton daughter nuclei. These results are displayed in Table III. For the  $^{22}\text{Al x}$  transitions, where the ordering is uncertain, a mass excess is calculated for each possibility. Also included in Table III are the excitation energies of these intermediate states (calculated using proton daughter masses from Ref. 13) and a column headed "known states" which contains excitation energies of known proton daughter states (from Ref. 14) with energies close enough to those observed to possibly be the intermediate state. It can be seen that for each observed intermediate state, there is a corresponding, previously

observed state (if the tentative ordering of the  $^{22}\text{Al}$  x transitions, as presented above, is accepted). This does not, of course, conclusively identify these previously known states as the two-proton intermediate states, but it is likely that this is the case for most of the transitions. Decay schemes based on the information presented in Table III are shown in Figs. 14 and 15.

Two-proton branching relative to that of single proton emission (2p/1p ratio) can be determined since, in addition to the two-proton coincidences, the detector systems used (see Section III) were also capable of detecting the higher energy (7-8 MeV) single proton groups of  $^{22}\text{Al}$  and  $^{26}\text{P}$ . These ratios are presented in Table IV. The single proton groups were observed with higher backgrounds than the measurements described in Refs. 2 and 3; however, since some concessions in telescope design were necessary to allow detection of low energy two-proton coincidences (primarily, thinner  $\Delta E$  were used detectors than were optimum for high energy proton detection). This is probably the largest source of error in this 2p/1p ratio, followed by uncertainties in two-proton to single proton detection efficiencies and low counting statistics. Due to low counting statistics, all two-proton coincidences for each isotope's decay were summed rather than attempting a treatment of individual transitions. These ratios were calculated relative to the most intense single proton group known in each decay (7.839 MeV for  $^{22}\text{Al}$  and 7.269 MeV for  $^{26}\text{P}$ , laboratory energies) with an isotropic sequential emission of the protons assumed.

Absolute errors on these ratios are difficult to determine, but the 2p/1p values shown are thought to be reliable to within 50%. For  $^{26}\text{P}$ , the 2p/1p ratio is close to unity and does not vary significantly from small to large angles.  $^{22}\text{Al}$  has a higher 2p/1p ratio; however, the  $^{22}\text{Al}$  large angle measurement is significantly larger than the small angle measurement. This, in itself, might be ascribed to uncertainties in the measurement technique, but, as discussed above, the large angle  $^{22}\text{Al}$  measurement has some other inconsistencies when compared to the observed spectrum at small angles. The most striking of these, is the possibility of a continuum type contribution to the  $^{22}\text{Al}$  x individual proton spectrum shown in Fig. 9b. The appearance of such a contribution at large angles would be very difficult to explain, given its absence at small angles (see Fig. 8b) but its presence could cause the variation in 2p/1p ratio shown in Table IV. It is possible that this observation is due to an unidentified detector effect associated with the general difficulties of these nanobarn level experiments, but the possibility that this is due to some more interesting physical phenomenon should not be excluded.

## V. Summary

Beta-delayed two-proton radioactivity has been observed for the two nuclei,  $^{22}\text{Al}$  and  $^{26}\text{P}$ . Two-proton coincidence experiments have been performed at small and large angles and have shown that the dominant two-proton emission mechanism is a sequential process. Possible decay schemes have been determined for each isotope. Some puzzling features of the large angle two-proton measurements for  $^{22}\text{Al}$  decay have been observed and suggest further investigation.

Future work on beta-delayed two-proton radioactivity in general will be directed towards discovering new isotopes exhibiting this decay mode; the higher  $T_z = -2$  nuclei  $^{46}\text{Mn}$  and  $^{50}\text{Co}$  are prime candidates. These studies may show that beta-delayed two-proton emission is not only an interesting phenomenon in itself, but may serve as a useful tool for detection and decay studies of new isotopes not observable by other techniques.

## Acknowledgements

We would like to thank J. Randrup for useful discussions of two-proton emission mechanisms and C. Maples, B. Rathbun, and D. Weaver for their help with the MIDAS computer system which was used in the data reduction.

TABLE I. Observed two-proton sum energies.

Two-proton group		Small angle measurement	Large angle measurement
22A1	x	4.14(2)	4.35(3)
22A1	g	5.64(2)	5.93(3)
26p	g	4.92(2)	5.15(4)



TABLE II. Observed individual proton energies.

---

22A1 x		x1	x1'	x2	x2'	x3	x3'
	small	1.88(2)	2.26(2)	1.66(2)	2.48(2)	1.48(2)	2.64(2)
22A1 g		g1	g1'	g2	g2'		
	small	2.62(3)	2.98(3)	1.50(3)	4.05(3)		
	large	2.61(3)	3.34(3)	1.82(3)	4.06(3)		
26p g		g1	g1'				
	small	1.21(2)	3.69(2)				
	large	1.52(3)	3.64(3)				

---

TABLE III. Calculated proton-daughter state mass excesses and excitations.

Precursor	Assumed $p_1$ group	Mass** Excess	$E_x$	Known*** States
22A1	$\left(\frac{x1'}{x1}\right)^*$	3.99(2) 4.39(2)	6.18(2) 6.58(2)	<u>6.170(30)</u> (1/2-7/2) <sup>+</sup>
22A1	$\left(\frac{x2'}{x2}\right)^*$	3.76(2) 4.62(2)	5.95(2) 6.81(2)	<u>5.979(15)</u> (1/2-7/2) <sup>+</sup>
22A1	$\left(\frac{x3'}{x3}\right)^*$	3.59(2) 4.81(2)	5.78(2) 7.00(2)	5.770(20) (1/2-7/2) <sup>+</sup> 7.060(30)
22A1	g1	3.62(3)	5.81(3)	5.770(20) (1/2-7/2) <sup>+</sup> 5.815 7/2 <sup>-</sup>
22A1	g2'	2.11(3)	4.30(3)	4.294(3) 5/2 <sup>+</sup>
26p	g1	-5.20(2)	3.72(2)	3.6957(5) (7/2 <sup>-</sup> )

\*Ordering is uncertain. Underlined group is the more probable candidate.

\*\*Calculated using small angle values.

\*\*\*Known states from Ref. 14 that are close enough in energy to be possible intermediate states.

TABLE IV.  $2p/1p$  ratios

Isotope	Small angles	Large angles
$^{22}\text{Al}$	1.9	5.5
$^{26}\text{p}$	0.9	1.4

Footnotes and References

+Present address: Dept. of Physics, University of Jyvaskyla, Finland.

++Present address: Dept. of Physics, Nanjing University, China.

1. V. I. Gol'danskii, Pis'ma Zh. Eksp. Teor. Fiz. 32, 572 (1980);  
JETP Lett. 32, 554 (1980).
2. M. D. Cable, J. Honkanen, R. F. Parry, H. M. Thierens, J.M.  
Wouters, Z. Y. Zhou, and J. Cerny, Phys. Rev. C26, 1778 (1982).
3. M. D. Cable, J. Honkanen, R. F. Parry, S. H. Zhou, Z. Y. Zhou,  
and J. Cerny, Phys. Lett. 123B, 25 (1983).
4. M. D. Cable, J. Honkanen, R. F. Parry, S. H. Zhou, Z. Y. Zhou,  
and J. Cerny, Phys. Rev. Lett. 50, 404 (1983).
5. J. Honkanen, M. D. Cable, R. F. Parry, S. H. Zhou, Z. Y. Zhou,  
and J. Cerny, Phys. Lett. 133B, 146 (1983).
6. V. I. Gol'danskii, Usp. Fiz. Nauk 87, 255 (1965); Sov. Phys. Usp.  
8, 770 (1966).
7. T. V. Congedo, I. S. Lee-Fan and B. L. Cohen, Phys. Rev. C22, 985  
(1980).
8. D. P. Stahel, Ph.D. Thesis, Lawrence Berkeley Laboratory, Rept.  
No. LBL-9706 (1979).

9. K. R. Symon, Mechanics, (Addison-Wesley, Reading, MA, 1971) p. 175.
10. G. G. Ohlsen, Nucl. Instr. and Meth. 37, 240 (1965).
11. L. C. Biedenharn in: Nuclear Spectroscopy, Part B, ed. F. Ajzenberg-Selove (Academic Press, New York, 1960) p. 732.
12. C. Maples and J. Sivak, IEEE Trans. Nucl. Sci. 26, 4409 (1979).
13. A. H. Wapstra, G. Audi, and K. Bos, January 1982 Atomic Mass Table for Nuclides.
14. P. M. Endt and C. van der Leun, Nucl. Phys. A310, 1 (1978).

Figure Captions

- Fig. 1. Proposed partial decay scheme for  $^{22}\text{Al}$ .
- Fig. 2. Proposed partial decay scheme for  $^{26}\text{P}$ .
- Fig. 3. Schematic diagram of helium jet apparatus. Small angle detector system is shown.
- Fig. 4. Schematic diagram of the small angle detector system.
- Fig. 5. Monte Carlo simulation of sequential emission of two protons as observed with the small angle detector system. See text.
- (a) Two-proton summed energy spectrum.
- (b) Individual proton energy spectrum. Peak heights are arbitrarily normalized to lower energy group for display purposes.
- Fig. 6. Monte Carlo simulation of  $^2\text{He}$  emission of two protons as observed with the small angle detector system. See text.
- (a) Two-proton summed energy spectrum.
- (b) Individual proton energy spectrum.
- Fig. 7. Schematic diagram of the large angle detector system.
- Fig. 8. Monte Carlo simulation of sequential emission of two protons as observed with the large angle detector system. See text.
- (a) Two-proton summed energy spectrum.
- (b) Individual proton energy spectrum. Peak heights are arbitrarily normalized to lower energy group for display purposes.
- Fig. 9. Proton-proton coincidence spectra obtained with the small angle detector system following the decay of  $^{22}\text{Al}$ . See text.
- (a) Two-proton summed energy spectrum. Groups x and g correspond to transitions involving the  $^{20}\text{Ne}$  first excited state and ground state, respectively. See Fig. 1.

(b) Individual proton energy spectrum for protons forming group x in part (a).

(c) Individual proton energy spectrum for protons forming group g in part (a).

Fig. 10. Proton-proton coincidence spectra obtained with the large angle detector system following the decay of  $^{22}\text{Al}$ . See text.

(a) Two-proton summed energy spectrum. Groups x and g correspond to transitions involving the  $^{20}\text{Ne}$  first excited state and ground state, respectively. See Fig. 1.

(b) Individual proton energy spectrum for protons forming group x in part (a).

(c) Individual proton energy spectrum for protons forming group g in part (a).

Fig. 11. Kinematic shift of  $^{22}\text{Al}$  two-proton peaks shown by overlaying Fig. 9a and 10a. Peak heights have been normalized to the small-angle measurement.

Fig. 12. Proton-proton coincidence spectra obtained with the small angle detector system following the decays of  $^{22}\text{Al}$  and  $^{26}\text{P}$ . See text.

(a) Two-proton summed energy spectrum containing both  $^{22}\text{Al}$  and  $^{26}\text{P}$  groups.

(b) Individual proton energy spectrum for protons from the  $^{26}\text{P}$  g group in part (a). This group corresponds to a transition to the  $^{24}\text{Mg}$  ground state (see Fig. 2).

Fig. 13. Proton-proton coincidence spectra obtained with the large angle detector system following the decays of  $^{22}\text{Al}$  and  $^{26}\text{P}$ .

See text.

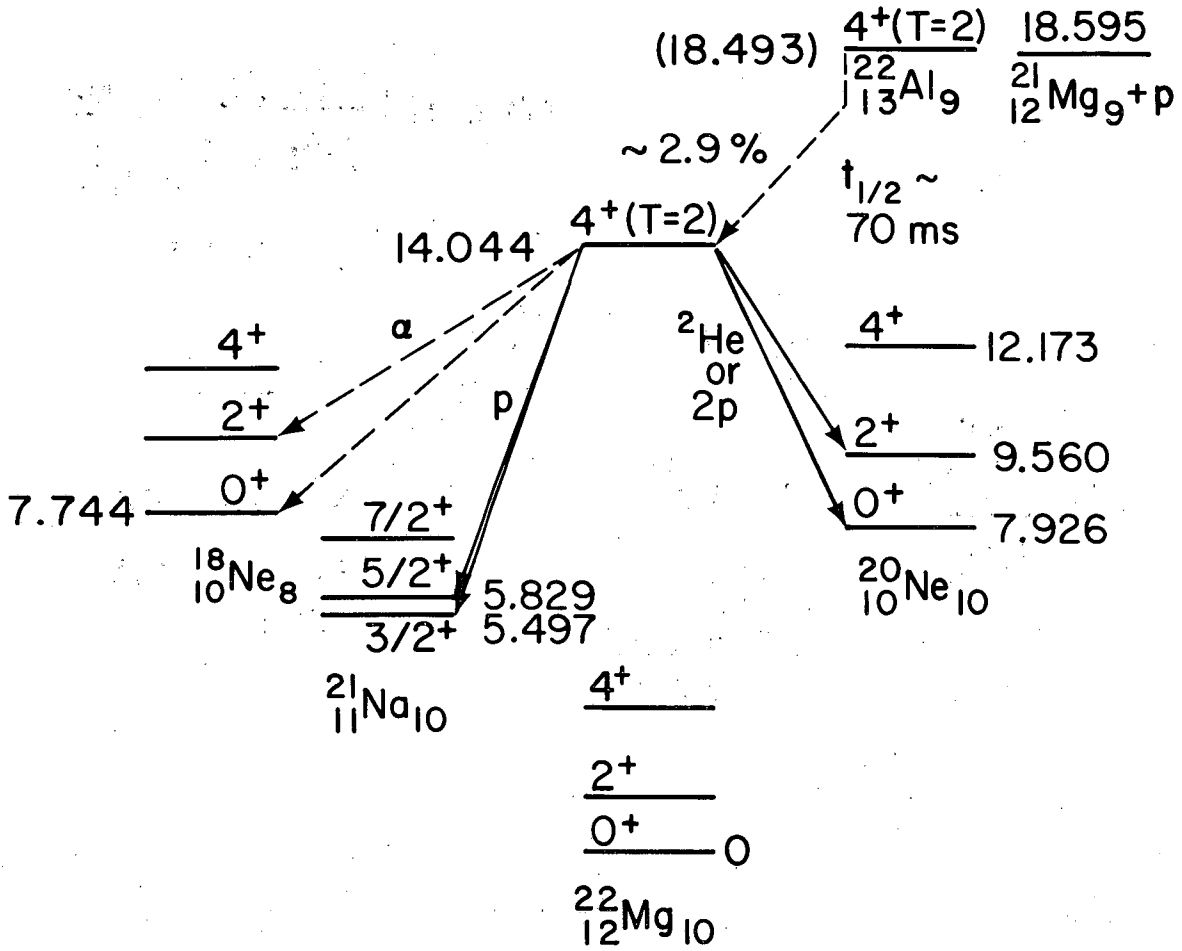
(a) Two-proton summed energy spectrum containing both  $^{22}\text{Al}$  and  $^{26}\text{P}$  groups.

(b) Individual proton energy spectrum for protons from the  $^{26}\text{P}$  g group in part (a). This group corresponds to a transition to the  $^{24}\text{Mg}$  ground state (see Fig. 2).

Fig. 14. Proposed new partial decay scheme for  $^{22}\text{Al}$ .

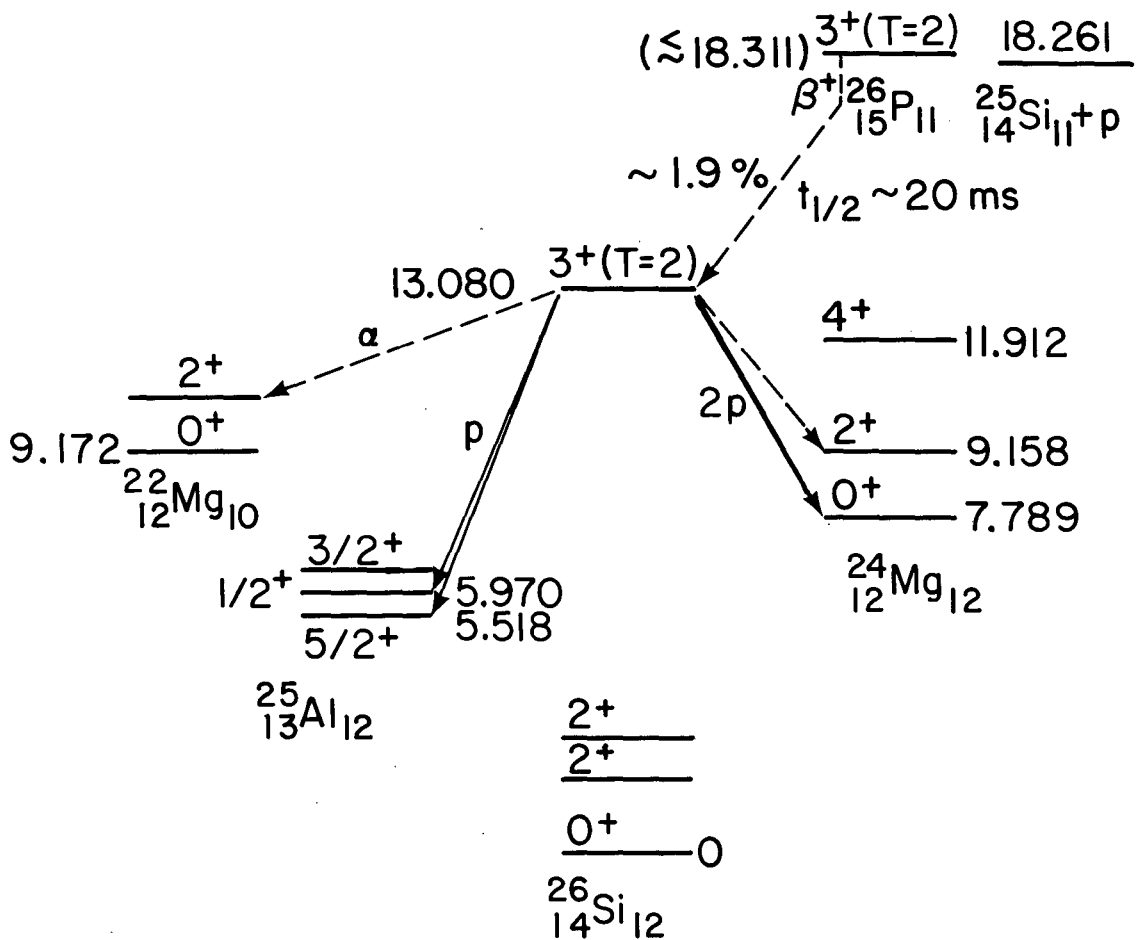
Fig. 15. Proposed new partial decay scheme for  $^{26}\text{P}$ .





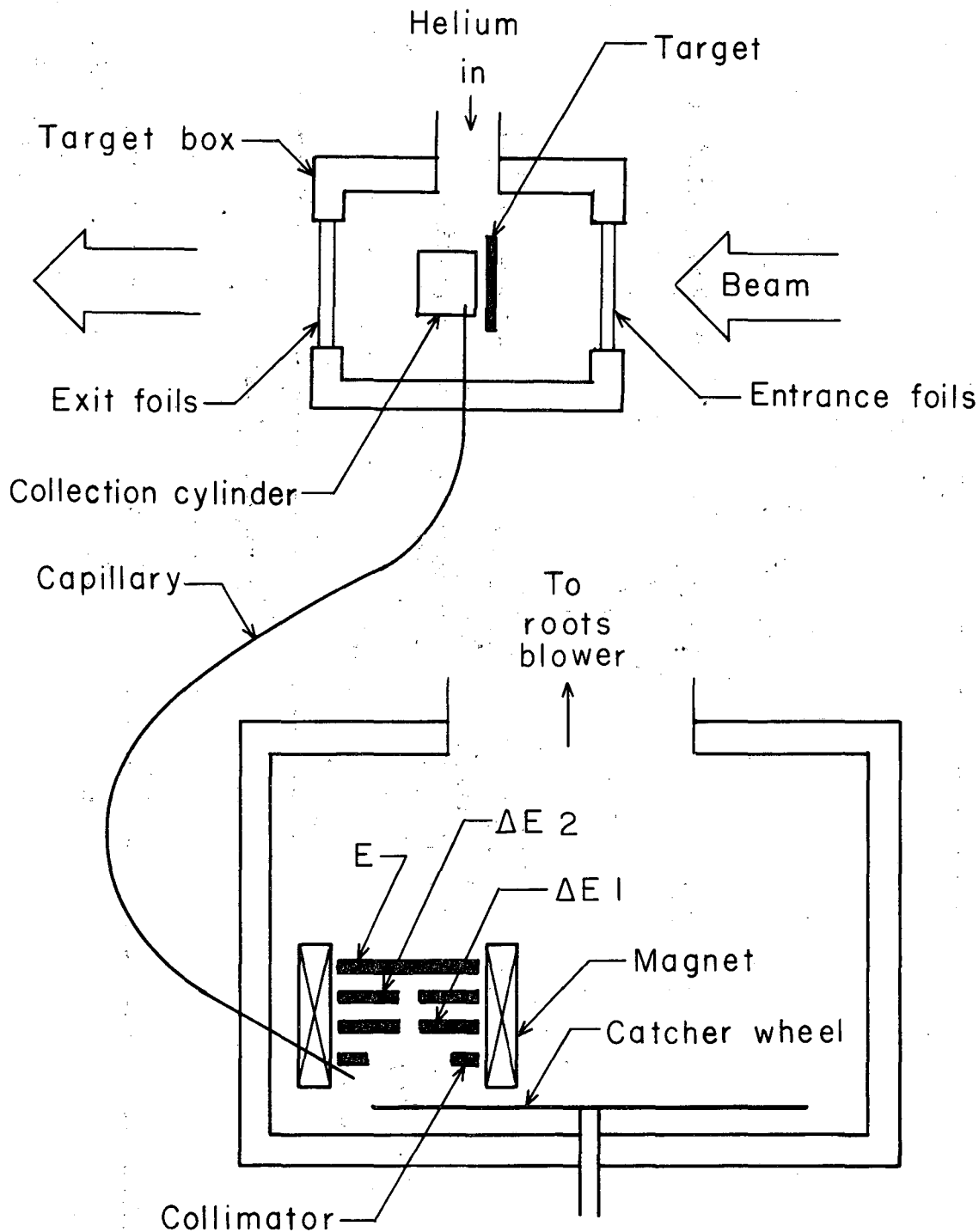
XBL 829-4626

Fig. 1



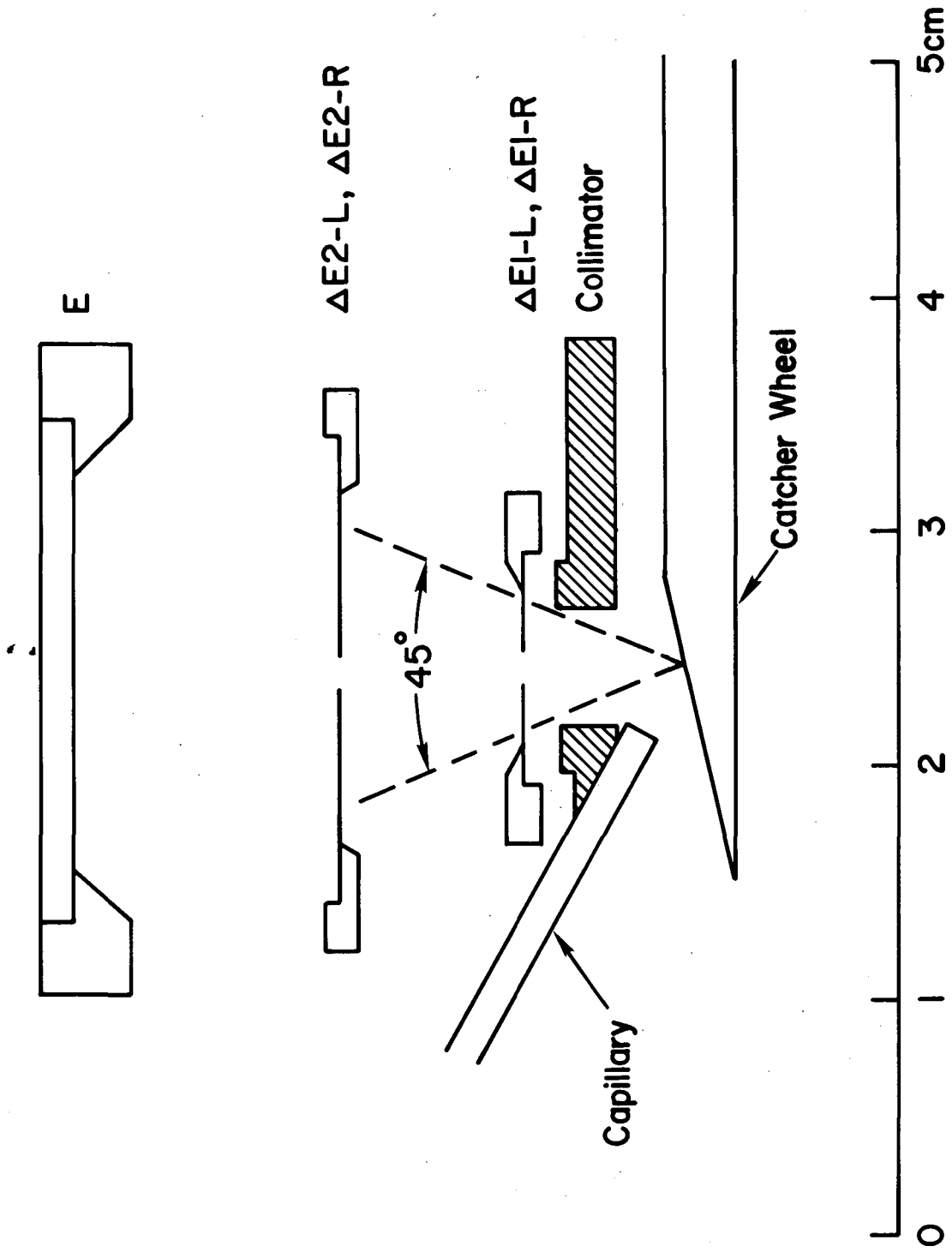
XBL 829-4628

Fig. 2



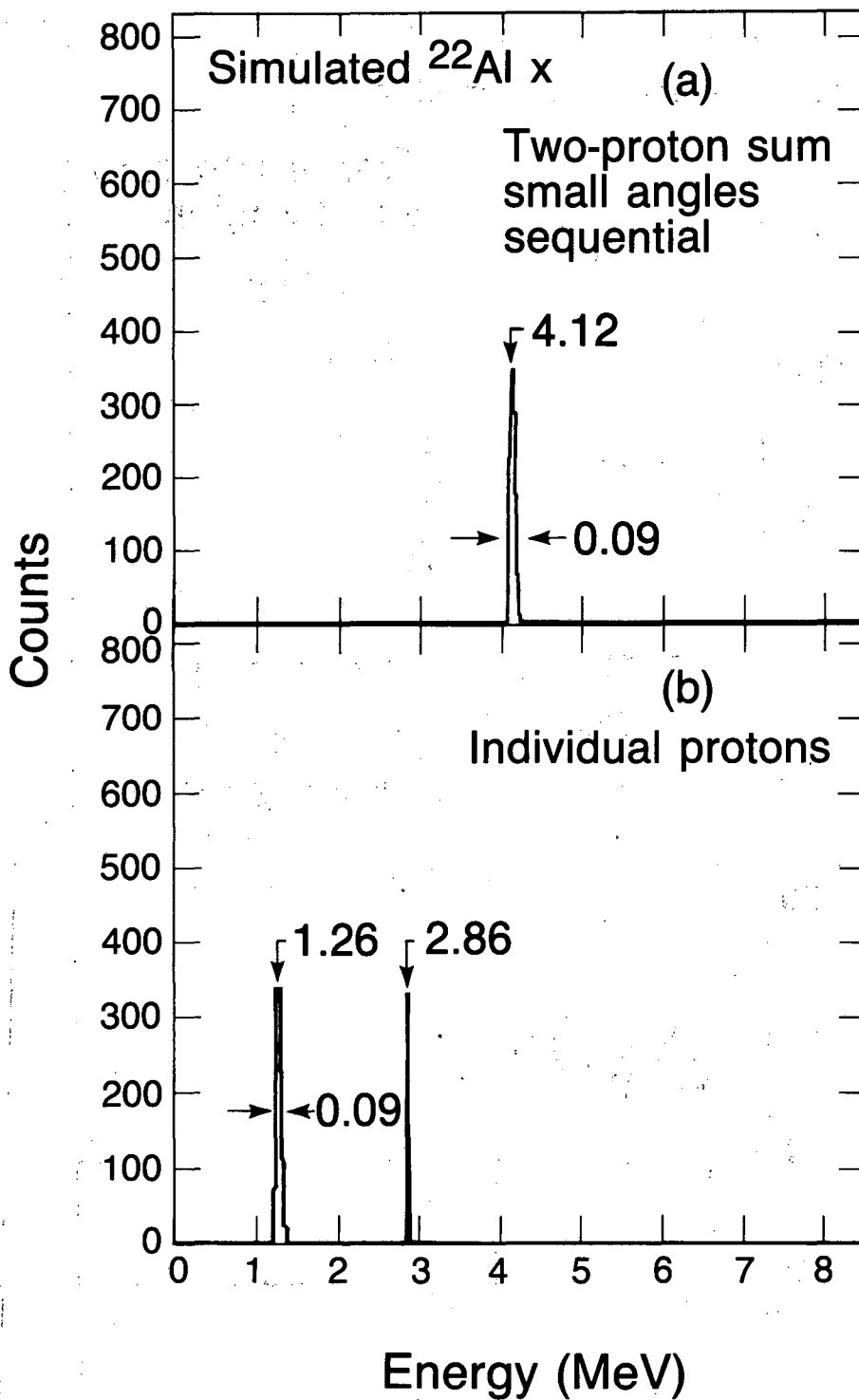
XBL 8212-12271

Fig. 3



XBL 842-10072

Fig. 4



XBL 843-10115

Fig. 5

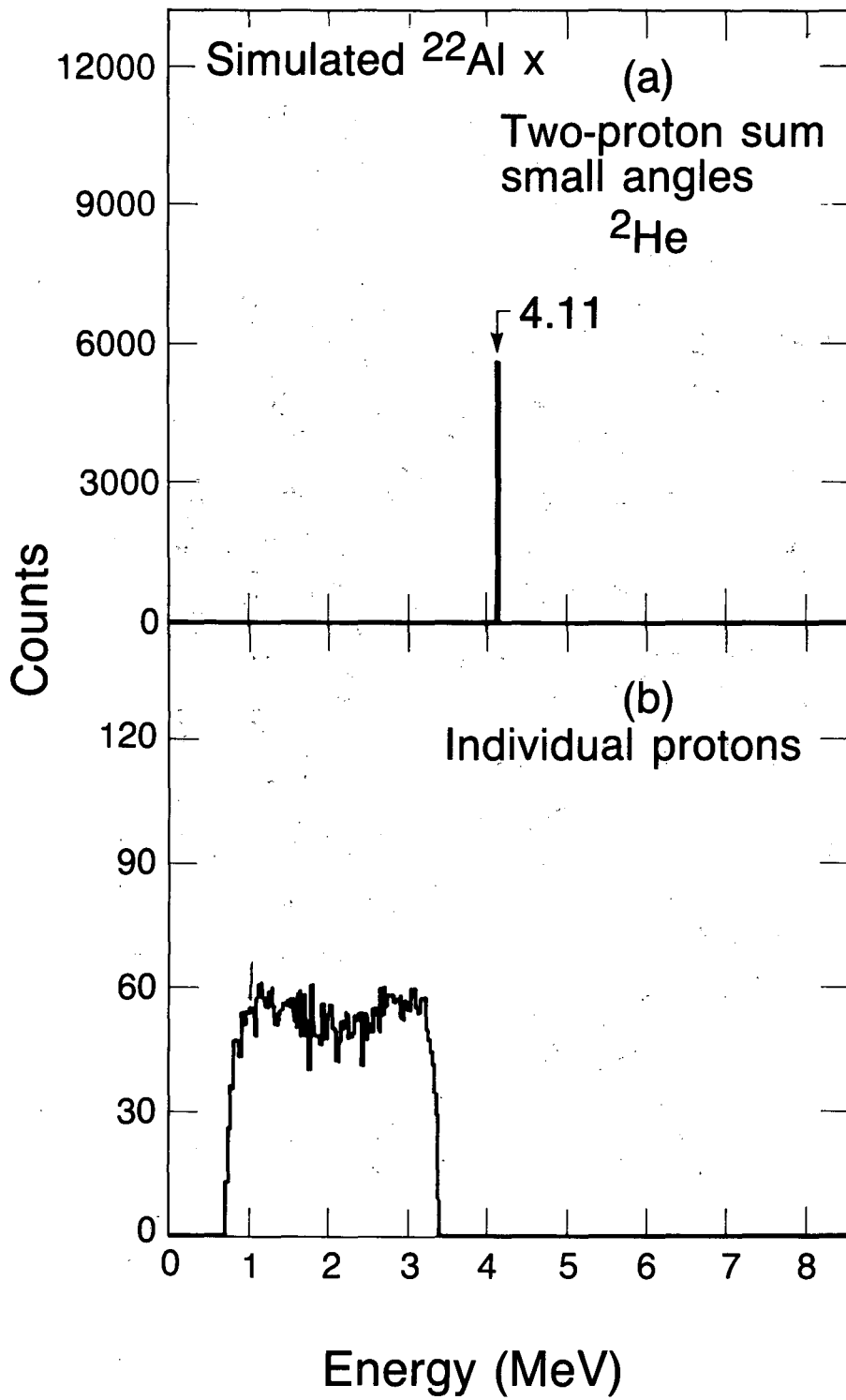
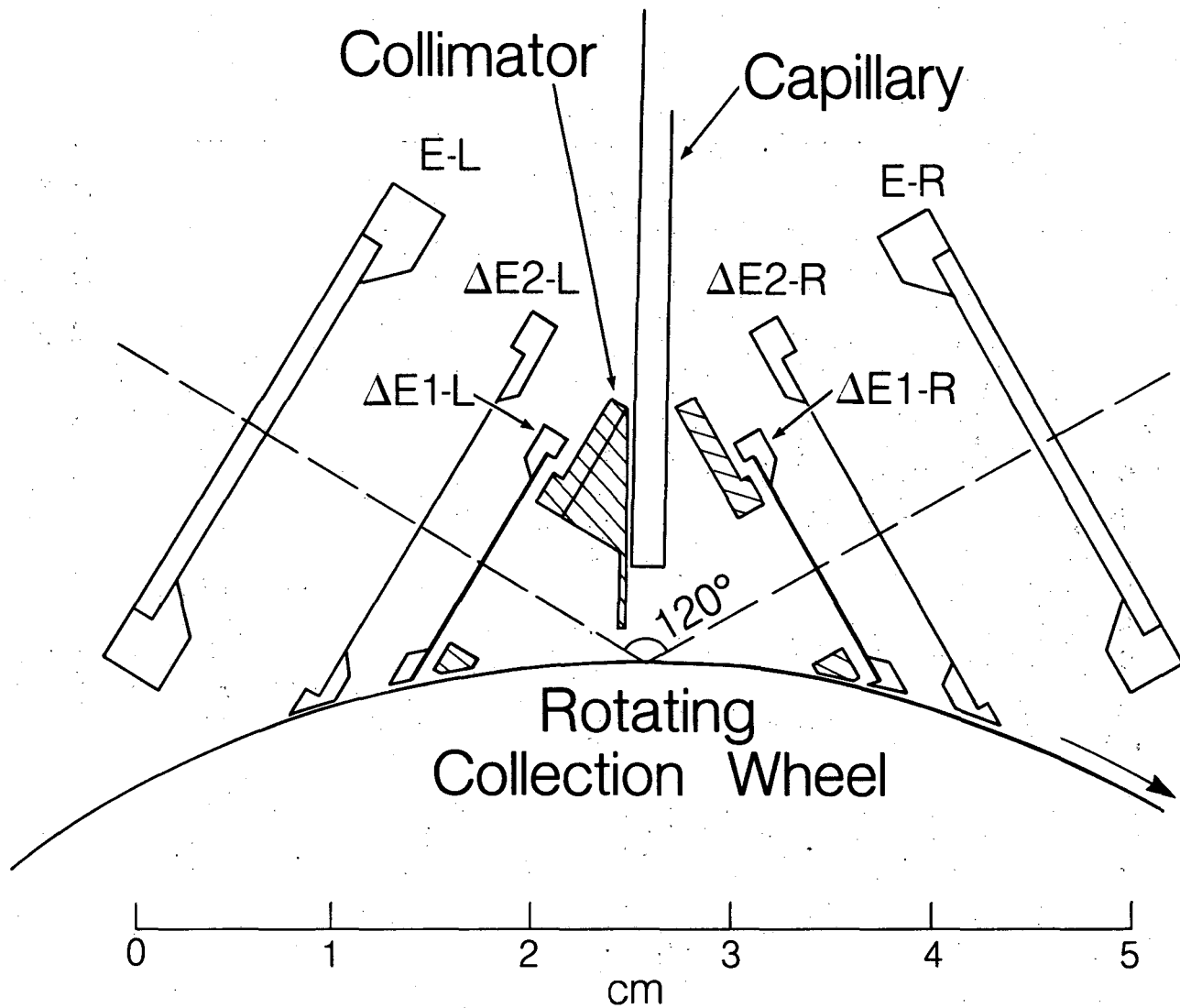


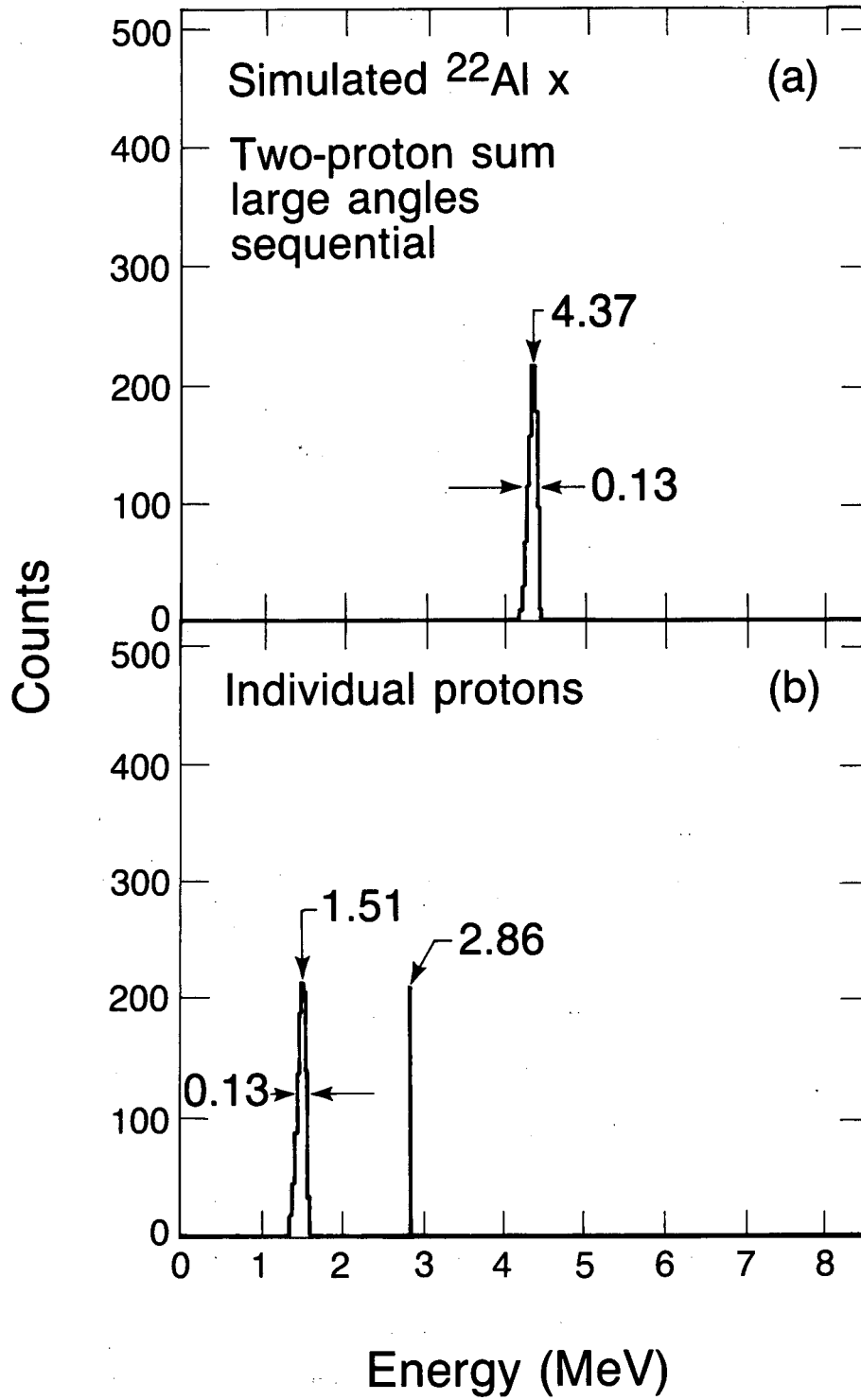
Fig. 6

XBL 843-10114



XBL 8311-6823

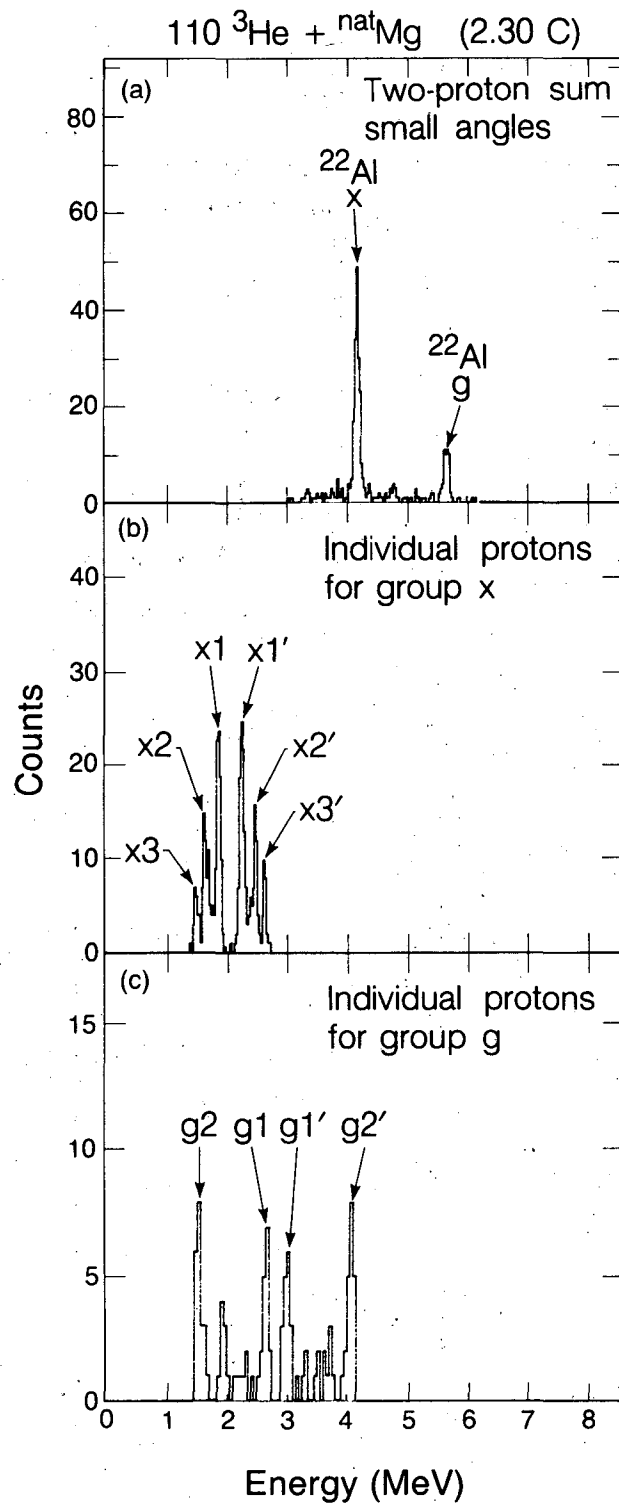
Fig. 7



XBL 843-10116

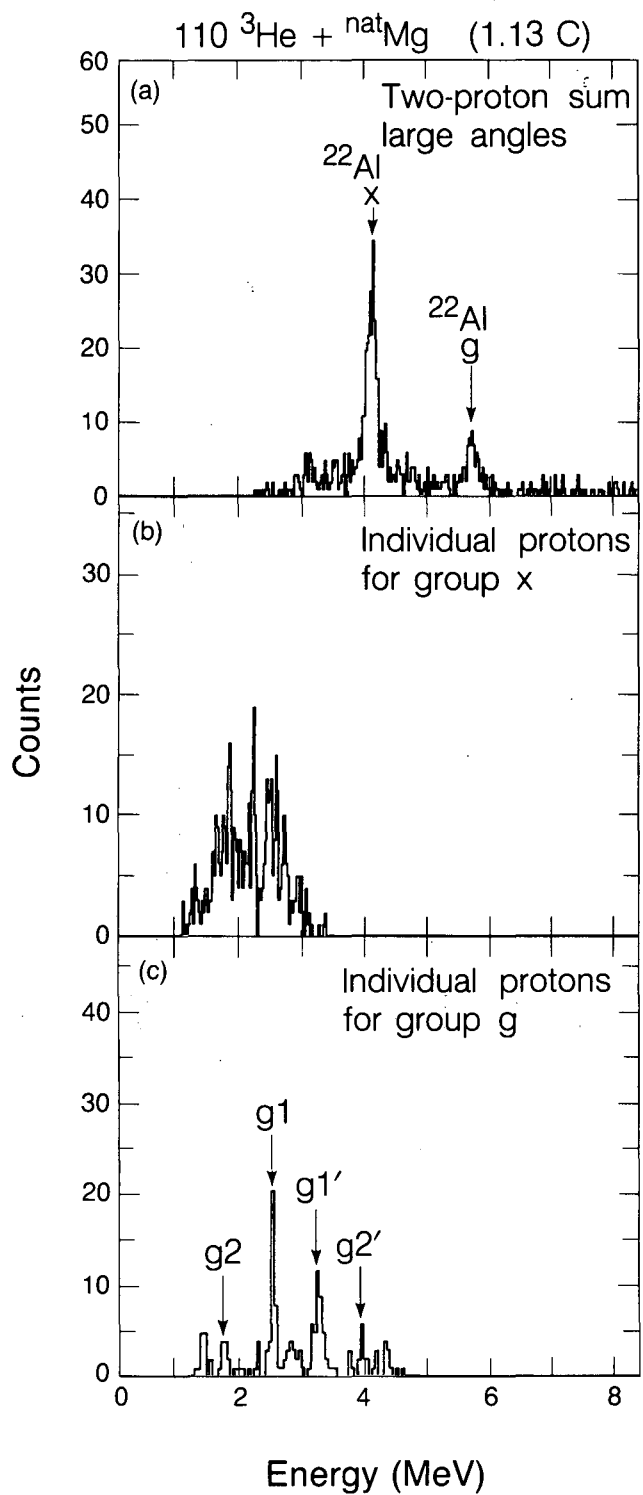
Fig. 8





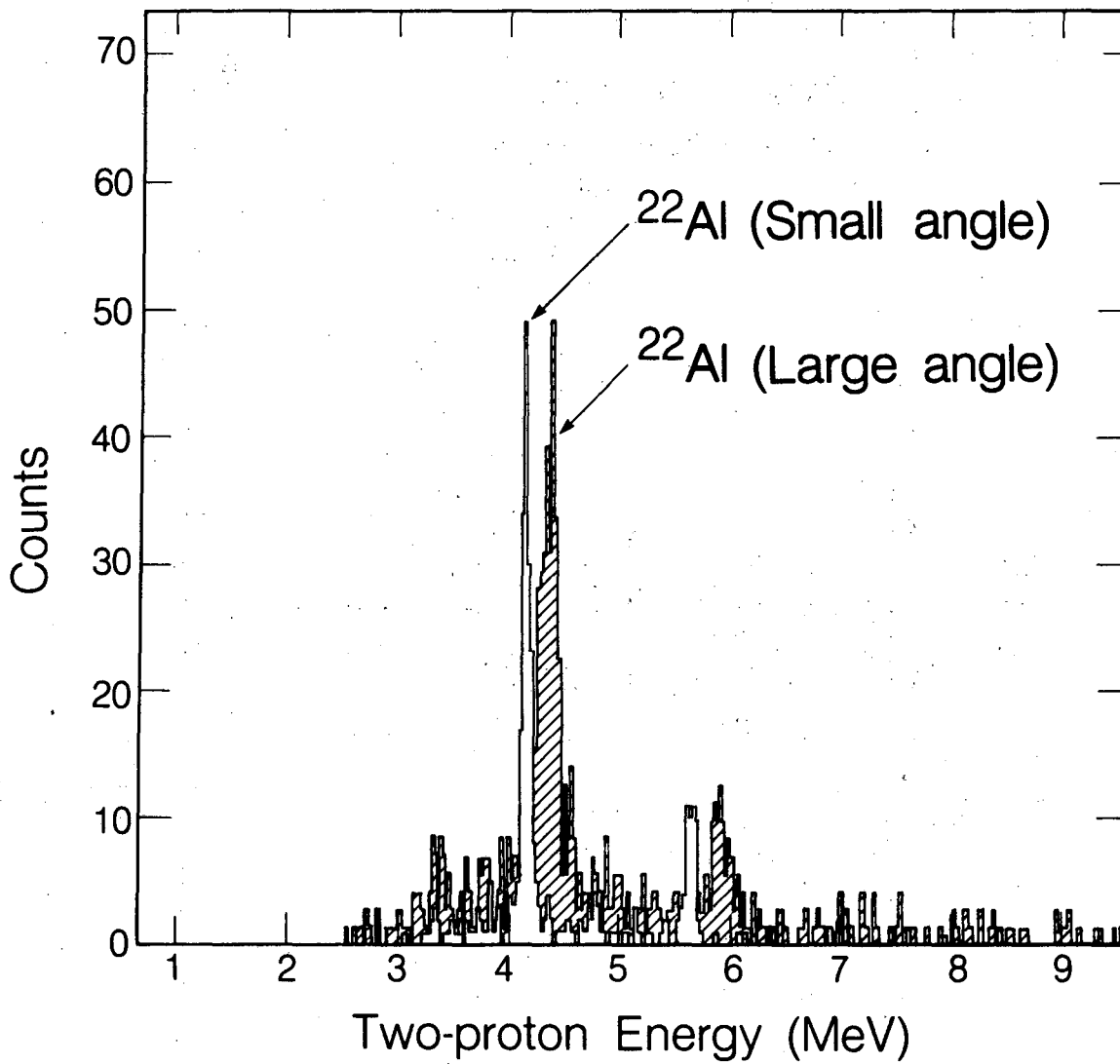
XBL 842-10071

Fig. 9



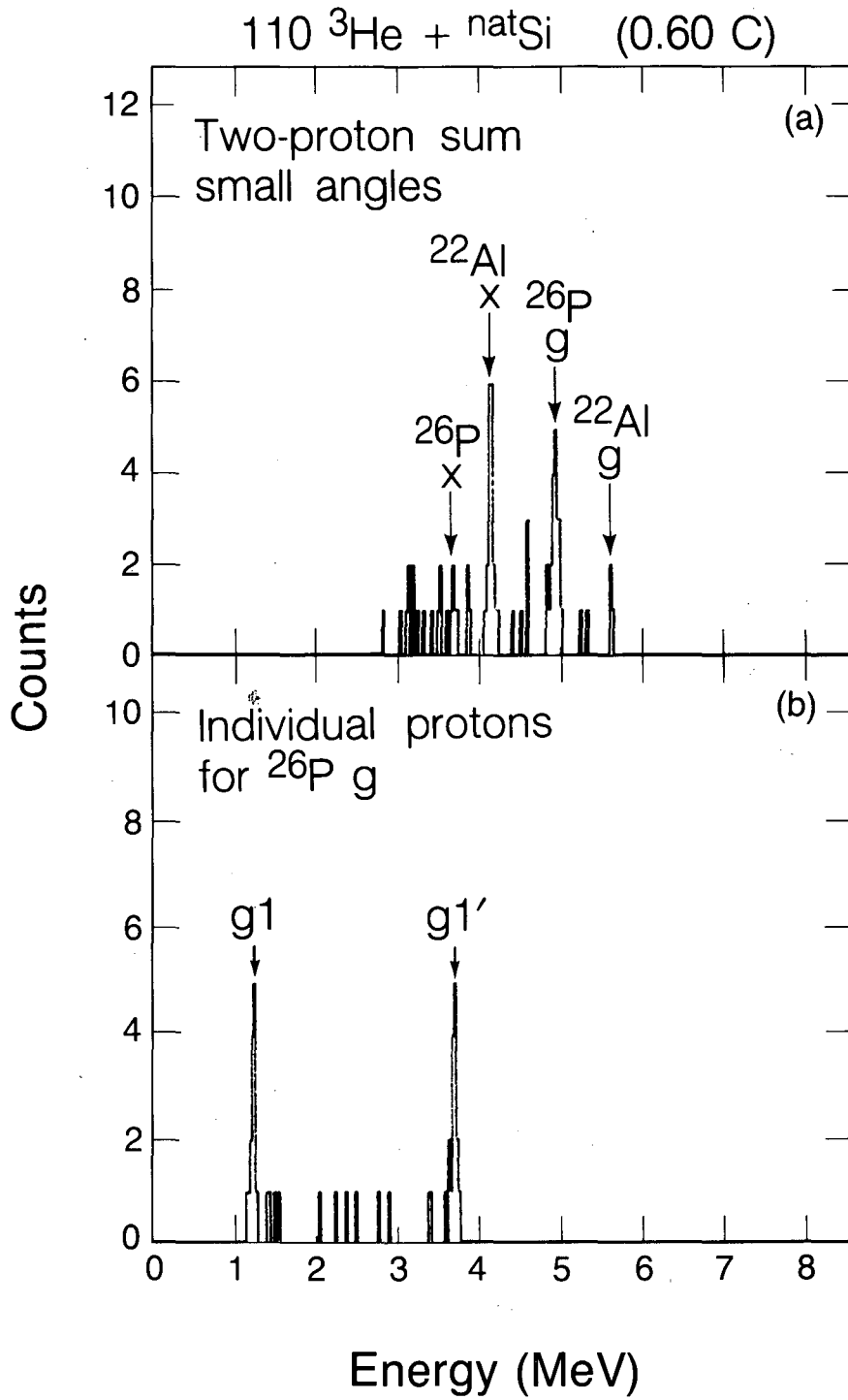
XBL 842-10064

Fig. 10



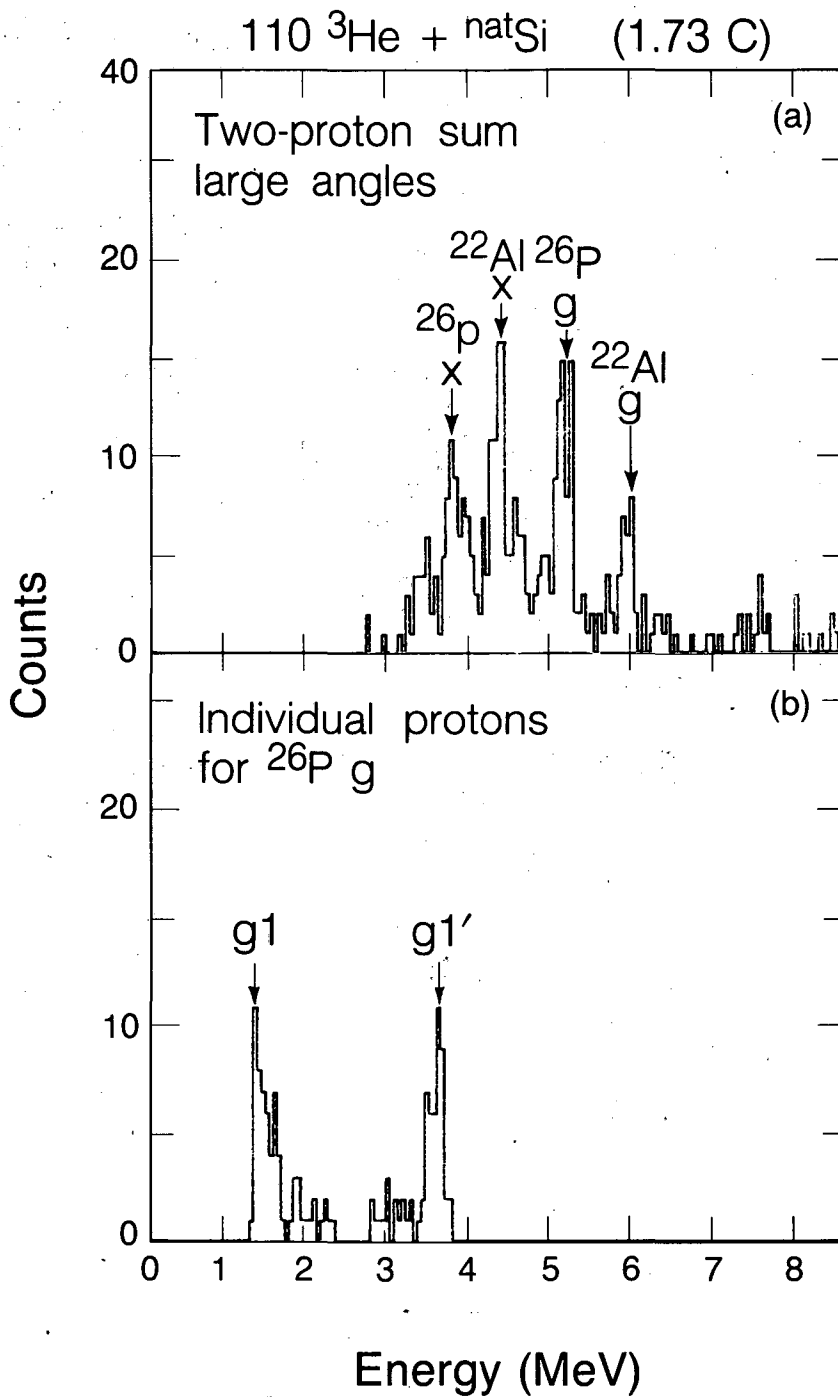
XBL 8312-2569

Fig. 11



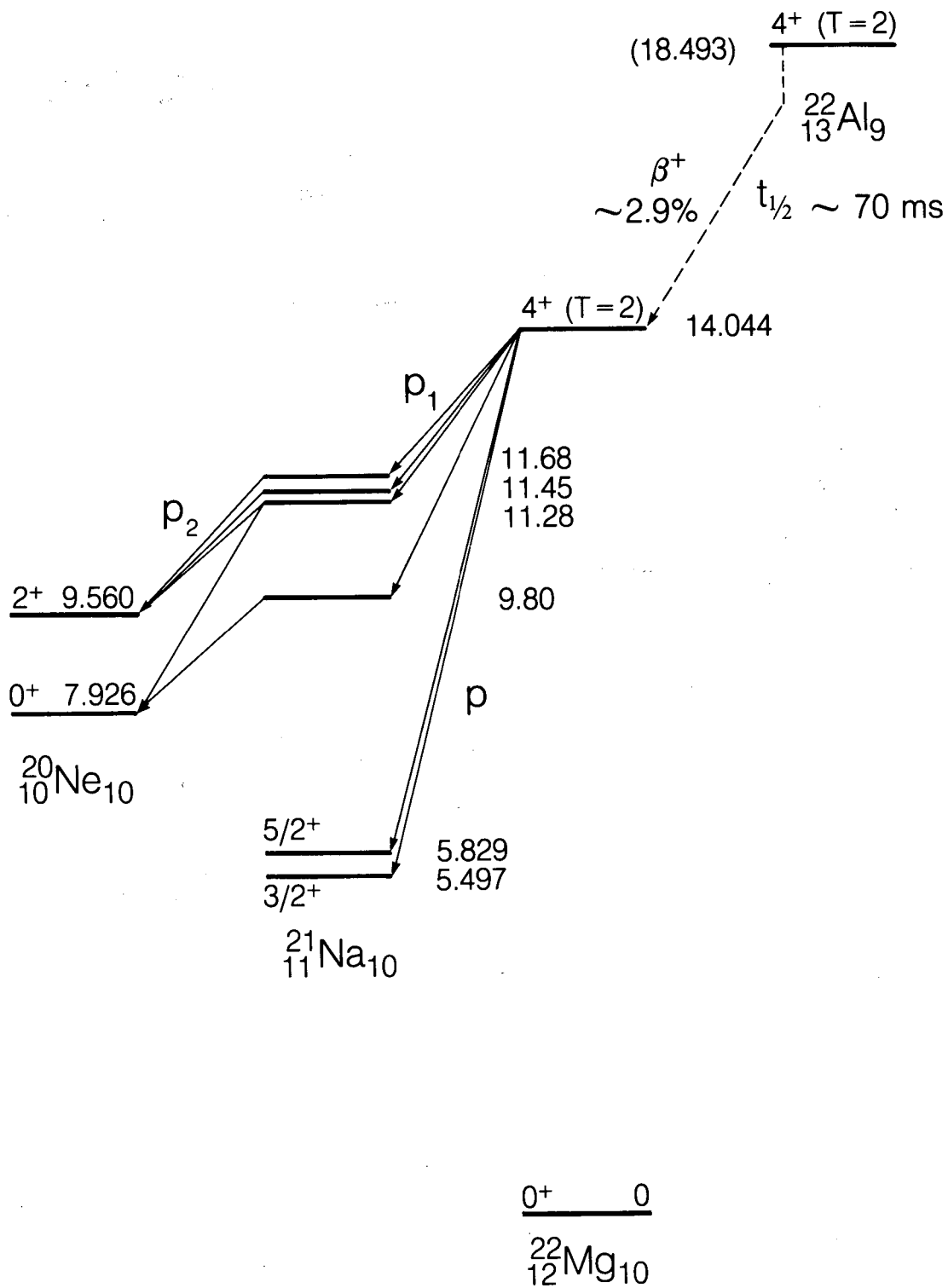
XBL 842-10070

Fig. 12



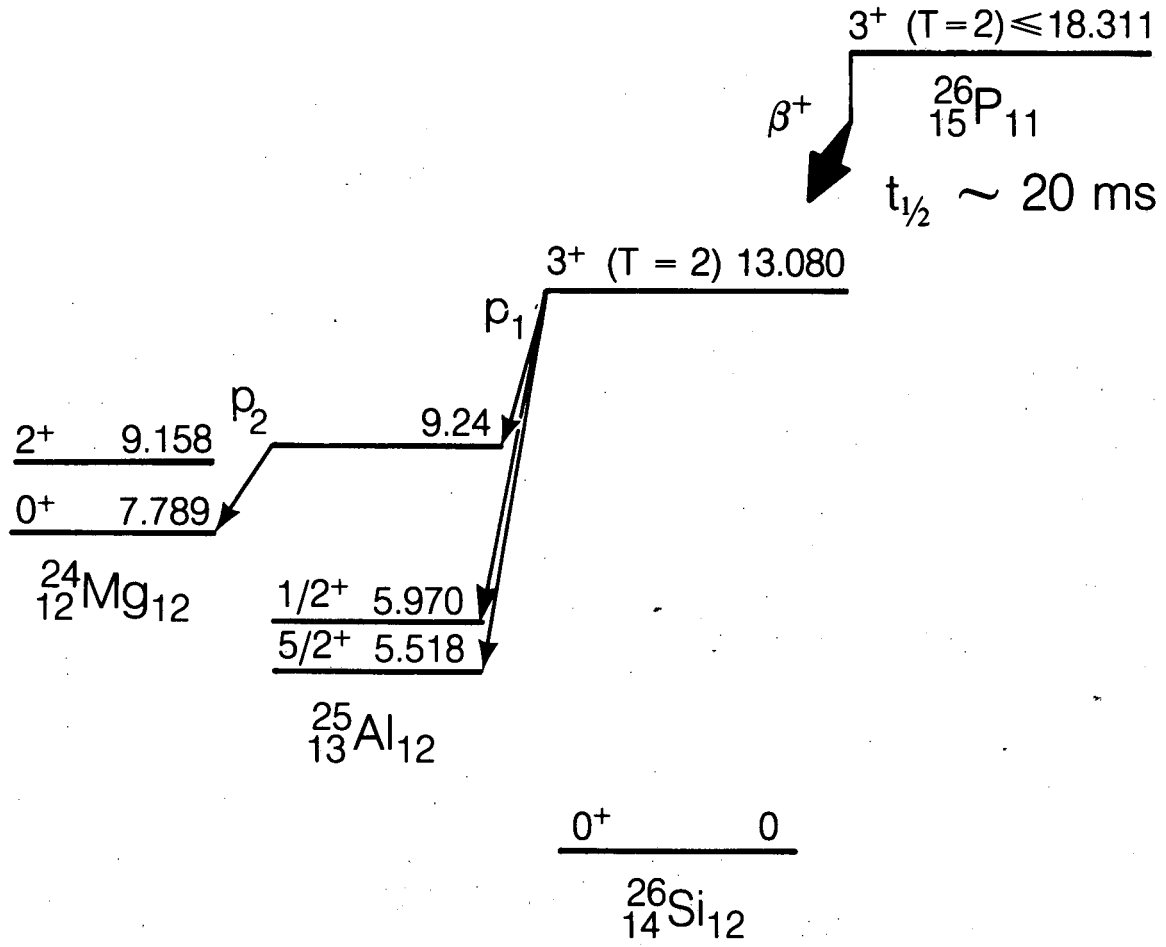
XBL 842-10065

Fig. 13



XBL 842-9422

Fig. 14



XBL 837-1889

Fig. 15

This report was done with support from the Department of Energy. Any conclusions or opinions expressed in this report represent solely those of the author(s) and not necessarily those of The Regents of the University of California, the Lawrence Berkeley Laboratory or the Department of Energy.

Reference to a company or product name does not imply approval or recommendation of the product by the University of California or the U.S. Department of Energy to the exclusion of others that may be suitable.



TECHNICAL INFORMATION DEPARTMENT  
LAWRENCE BERKELEY LABORATORY  
UNIVERSITY OF CALIFORNIA  
BERKELEY, CALIFORNIA 94720